Articles

(*E*)-Enolbutyryl-UDP-*N*-acetylglucosamine as a Mechanistic Probe of UDP-*N*-acetylenolpyruvylglucosamine Reductase (MurB)[†,‡]

Watson J. Lees,[§] Timothy E. Benson,[§] James M. Hogle, and Christopher T. Walsh*

Department of Biological Chemistry and Molecular Pharmacology, Harvard Medical School, Boston, Massachusetts 02115

Received September 25, 1995[⊗]

ABSTRACT: UDP-*N*-acetylenolpyruvylglucosamine reductase (MurB), a peptidoglycan biosynthetic enzyme from *Escherichia coli*, reduces both (*E*)- and (*Z*)-isomers of enolbutyryl-UDP-GlcNAc, C_4 analogs of the physiological C_3 enolpyruvyl substrate, to UDP-methyl-*N*-acetylmuramic acid in the presence of NADPH. The X-ray crystal structure of the (*E*)-enolbutyryl-UDP-GlcNAc−MurB complex is similar to that of the enolpyruvyl-UDP-GlcNAc−MurB complex. In both structures the groups thought to be involved in hydride transfer to C3 and protonation at C2 of the enol ether substrate are arranged *anti* relative to the enol double bond. The stereochemical outcome of reduction of (*E*)-enolbutyryl-UDP-GlcNAc by NADPD in D_2O is thus predicted to yield a (2*R*,3*R*)-dideuterio product. This was validated by conversion of the 2,3-dideuterio-UDP-methyl-*N*-acetylmuramic acid product to 2,3-dideuterio-2-hydroxybutyrate, which was shown to be (2*R*) by enzymatic analysis and (3*R*) by NMR comparison to authentic (2*R*,3*R*)- and (2*R*,3*S*)-2,3-dideuterio-2-hydroxybutyrate. Remarkably, the (*E*)-enolbutyryl-UDP-GlcNAc was found to partition between reduction to UDP-methyl-*N*-acetylmuramic and isomerization to the (*Z*)-substrate isomer in the MurB active site, indicative of a C2 carbanion/enol species that is sufficiently long-lived to rotate around the C2−C3 single bond during catalysis.

Interest in new inhibitors of bacterial cell wall biosynthesis has increased as bacteria have developed resistance to currently known antibiotics. An important approach in rational design of new inhibitors is to investigate the structure and reaction mechanism of the enzymes involved in unique and essential bacterial pathways. We have been investigating the first two committed steps of peptidoglycan biosynthesis, which are catalyzed by the enzymes MurA and MurB. MurA (formerly named MurZ) catalyzes the transfer of an enolpyruvyl group from phosphoenolpyruvate (PEP)[1] to the 3′-hydroxyl of UDP-GlcNAc, generating enolpyruvyl-UDP-GlcNAc (Brown et al., 1995) (Figure 1). MurB catalyzes the NADPH-dependent reduction of enolpyruvyl-UDP-GlcNAc, forming UDP-MurNAc (Benson et al., 1993). Subsequently, other enzymes in the pathway catalyze the sequential addition of three amino acids and then a dipeptide. The resulting UDP-MurNAc pentapeptide is then activated for incorporation into the bacterial cell wall.

The proposed mechanism of MurB begins with the binding of NADPH to the enzyme and hydride transfer of the 4-*pro*-S hydrogen of NADPH to N5 of an enzyme-bound flavin (Figure 2) (Benson et al., 1993). Release of $NADP^+$ is followed by the binding of EP-UDP-GlcNAc (Dhalla et al., 1995). Hydride transfer from the reduced flavin to C3 of the enolpyruvyl moiety of the UDP-sugar substrate generates a carbanion equivalent at C2, which can be stabilized by the α-carboxylate at C1 as an enol intermediate. A solvent-equilibrated proton is then transferred to C2, giving the UDP-MurNAc product. Supporting this proposal, the new C3 hydrogen of UDP-MurNAc was shown to be derived from NADPH and the C2 hydrogen was shown to be derived from solvent (Benson et al., 1993). The proposed sequence of events is also consistent with ping-pong steady-state kinetics (Dhalla et al., 1995).

[†] This work was supported in part by National Institutes of Health Grant GM49338-02 (C.T.W.) and the W. M. Keck Foundation (J.M.H.). W.J.L. was supported by a postdoctoral fellowship from the Natural Sciences and Engineering Research Council of Canada.

[‡] The coordinates for the (*E*)-EB-UDP-GlcNAc−MurB complex have been deposited in the Brookhaven Protein Data Bank (ID Code 1MBB).

* To whom correspondence should be addressed.

[§] Both authors contributed equally to this work.

[⊗] Abstract published in *Advance ACS Abstracts,* January 15, 1996.

[1] Abbreviations: CI, chemical ionization; D-LDH, D-lactate dehydrogenase; (*E*)-EB-UDP-GlcNAc, uridine 5′-(trihydrogen diphosphate) *P*′-[2-(acetylamino)-3-*O*-((*E*)-1-carboxyprop-1-enyl)-2-deoxy-α-D-glucopyranosyl] ester; (*Z*)-EB-UDP-GlcNAc, uridine 5′-(trihydrogen diphosphate) *P*′-[2-(acetylamino)-3-*O*-((*Z*)-1-carboxyprop-1-enyl)-2-deoxy-α-D-glucopyranosyl] ester; FAB, fast atom bombardment; FAD, flavin adenine dinucleotide; EP-UDP-GlcNAc, uridine 5′-(trihydrogen diphosphate) *P*′-[2-(acetylamino)-3-*O*-((*E*)-1-carboxyeth-1-enyl)-2-deoxy-α-D-glucopyranosyl] ester; HEPES, 4-(2-hydroxyethyl)-1-piperazineethanesulfonic acid; HPLC, high-performance liquid chromatography; HRMS, high-resolution mass spectrum; L-LDH, L-lactate dehydrogenase; *m*/*e*, mass to charge ratio; NAD^+, oxidized β-nicotinamide dinucleotide; NADD, (4*R*)-[^{2}H]-reduced β-nicotinamide dinucleotide; $NADP^+$, oxidized β-nicotinamide dinucleotide phosphate; NADPD, (4*S*)-[^{2}H]-reduced β-nicotinamide dinucleotide phosphate; NADPH, reduced β-nicotinamide dinucleotide phosphate; NMR, nuclear magnetic resonance; (*E*)-PEB, (*E*)-phosphoenol-2-ketobutyrate; (*Z*)-PEB, (*Z*)-phosphoenol-2-ketobutyrate; PEG, poly(ethylene glycol); PEP, phosphoenolpyruvate; UDP-GlcNAc, uridine 5′-(trihydrogen diphosphate) *P*′-[2-(acetylamino)-2-deoxy-α-D-glucopyranosyl] ester; UDP-Me-MurNAc, uridine 5′-(trihydrogen diphosphate) *P*′-[2-(acetylamino)-3-*O*-(1(*R*)-carboxypropyl)-2-deoxy-α-D-glucopyranosyl] ester; UDP-MurNAc, uridine 5′-(trihydrogen diphosphate) *P*′-[2-(acetylamino)-3-*O*-(1(*R*)-carboxyethyl)-2-deoxy-α-D-glucopyranosyl] ester.

0006-2960/96/0435-1342$12.00/0

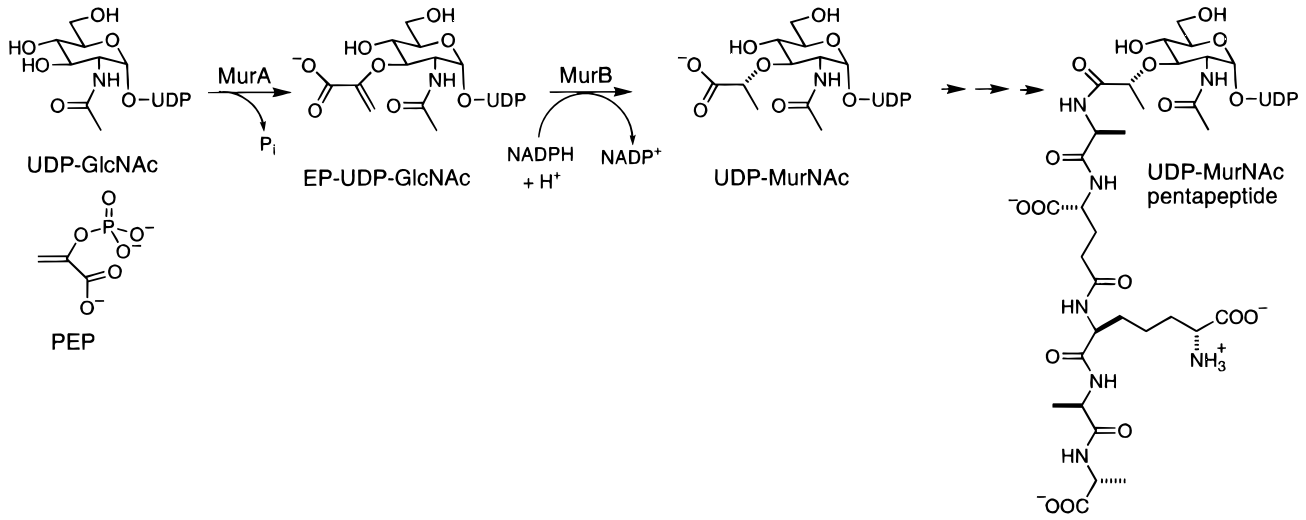

FIGURE 1: Enzymatic biosynthesis of UDP-*N*-acetylmuramic acid.

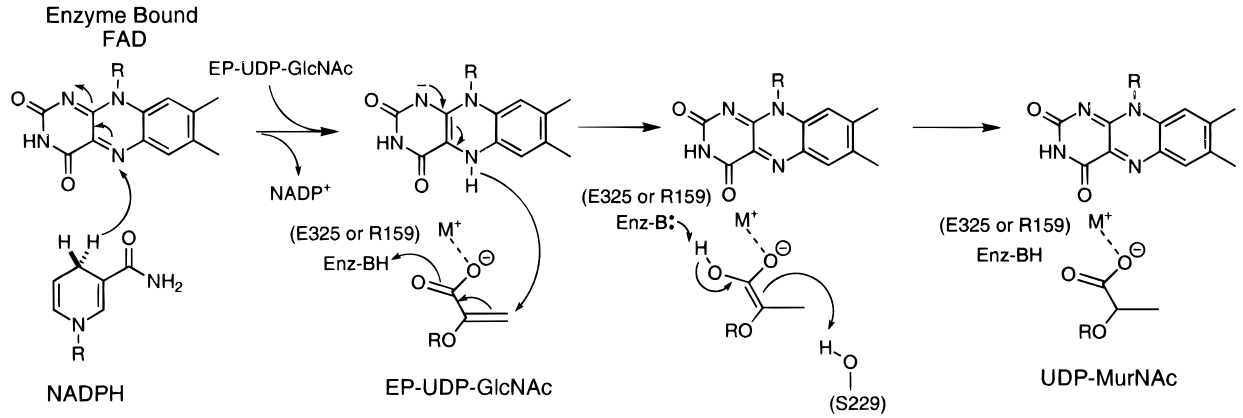

FIGURE 2: Proposed mechanism for reduction of EP-UDP-GlcNAc by MurB (Benson et al., 1993).

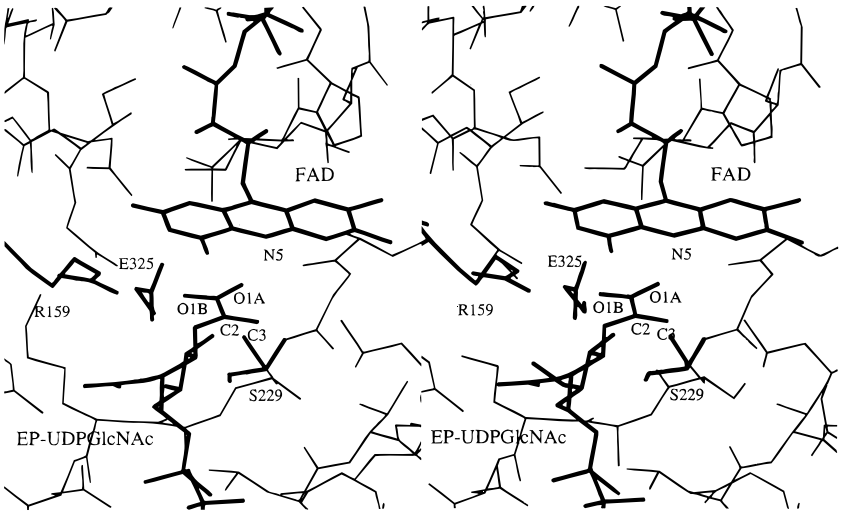

FIGURE 3: Active site of the EP-UDP-GlcNAc−MurB complex.

We recently reported the X-ray crystal structure of the EP-UDP-GlcNAc-MurB complex at 2.7 Å resolution (Benson et al., 1995). MurB is a mixed $\alpha + \beta$ protein comprised of three domains: domains 1 and 2 are involved in flavin binding while domain 3 is involved in substrate binding. The enzyme−substrate complex reveals three key residues and a monovalent cation potentially involved in catalysis (Figure 3). Both Glu-325 and Arg-159 are situated in close proximity to an oxygen of the enolpyruvylcarboxylate and are proposed to stabilize the enol intermediate by protonation. The monovalent cation is proposed to stabilize the other oxygen of the carboxylate. In the plane just below the C2−C3 bond, the Ser-229 hydroxyl is poised as the proton donor for quenching of the enol intermediate. In addition, the

Table 1: X-ray Crystallographic Data Collection and Refinement Statistics[a]

	resolution (Å)								
	12.0−5.80	4.37	3.65	3.19	2.88	2.64	2.45	2.30	12.0−2.3
R_{sym}[b]	0.036	0.040	0.047	0.071	0.103	0.145	0.193	0.260	0.072
no. of measurements	2778	6208	7946	8743	8697	6858	5863	5409	52502
no. of unique reflections	973	1376	1682	1921	2143	2212	2302	2326	14935
I/σ	16.8	17.2	13.9	10.8	7.5	5.3	4.1	3.1	10.0
completeness (%)	98.7	99.1	100.0	99.6	99.8	95.2	91.9	87.7	94.9
multiplicity	2.9	4.5	4.7	4.6	4.1	3.1	2.5	2.3	3.5

	crystallographic *R* factor[c]	free *R* factor[d]	no. of reflections
12.0−2.3 Å, all data	0.238	0.324	14834
8.0−2.3 Å, $F > 2\sigma$	0.221	0.311	14040

rms deviations	bonds 0.012 Å	angles 2.68°	
av *B* factor	main-chain atoms 14.3	side-chain atoms 15.6	FAD atoms 5.20	(*E*)-EB-UDP-GlcNAc atoms 9.91

[a] Data collection statistics were calculated in AGROVATA from the CCP4 package. Refinement statistics were calculated from X-PLOR. Model includes 340 residues, 119 water molecules, FAD, and (*E*)-EB-UDP-GlcNAc (2871 non-hydrogen atoms). [b] $R_{sym} = \sum_{i,(h,k,l)}|I_{i,(h,k,l)} - \langle I_{(h,k,l)}\rangle|/\sum_{i,(h,k,l)}\langle I_{(h,k,l)}\rangle$, where $\langle I_{(h,k,l)}\rangle$ is the statistically weighted average intensity of symmetry equivalent reflections. [c] Crystallographic *R* factor $= \sum_{(h,k,l)\epsilon T}||F_o| - |F_c||/\sum_{(h,k,l)\epsilon T}|F_o|$. [d] Free *R* factor $= \sum_{(h,k,l)\epsilon T}||F_o| - |F_c||/\sum_{(h,k,l)\epsilon T}|F_o|$, where *T* is a test set containing a randomly selected 10% of the observations omitted from the refinement process.

crystal structure predicts that the hydride is transferred from N5 of the FAD to the *re* face (determined from C2) of the C2−C3 bond of the enolpyruvyl moiety.

In order to verify the predicted stereochemistry of reduction by MurB, we utilized a substrate that would yield a product with a chiral center at C3. Recently, we demonstrated that both (*E*)- and (*Z*)-enolbutyryl-UDP-*N*-acetylglucosamine (EB-UDP-GlcNAc) can be generated from (*E*)- and (*Z*)-phosphoenolbutyrate (PEB) using MurA (Lees & Walsh, 1995). In this report we show that both (*E*)- and (*Z*)-EB-UDP-GlcNAc are substrates for MurB. Reduction of (*E*)-EB-UDP-GlcNAc with MurB in the presence of NADPD in D_2O followed by chemical decomposition has allowed us to determine the stereochemistry of hydride addition at C3 and protonation at C2. Enzyme-catalyzed isomerization of (*E*)- to (*Z*)-EB-UDP-GlcNAc provided the opportunity to further probe the mechanism of MurB.

EXPERIMENTAL PROCEDURES

General Methods and Materials. Ion-exchange resin AG 50W-X8 (100−200 mesh) was purchased from Bio-Rad Laboratories. MurB was purified as reported previously (Benson et al., 1993). The rate of reduction of (*E*)-EB-UDP-GlcNAc by MurB was determined using a continuous spectrophotometric assay (Benson et al., 1993). ^{1}H NMR spectra were obtained at 400 or 500 MHz. ^{13}C NMR spectra were obtained at 100 MHz. Proton chemical shifts were referenced to HOD set at 4.8 ppm. Carbon chemical shifts were referenced to an external standard of dioxane set at 67.6 ppm. The pD was measured by correcting the pH meter reading in D_2O by 0.4 unit (pD = pH meter reading + 0.4). An extinction coefficient at 262 nm of 10^4 M^{-1} cm^{-1} was used for all UDP sugars.

Analytical reversed-phase HPLC was performed on a Vydac C_{18} peptide and protein column with a flow rate of 1 mL/min {$HCOO^-(NH_4)^+$ [50 mM, pH 4.7]}. The effluent was monitored at 262 nm. Analytical and preparative anion-exchange HPLC were performed on a Pharmacia Mono Q (5/5) column with a flow rate of 2 mL/min of triethylamine bicarbonate, pH 8, using either routine 1, which was a linear gradient from 20 to 500 mM over 10 min after a 1 min initial wash, or routine 2, which was a linear gradient from 20 to 300 mM over 20 min after a 1 min initial wash. Preparative reversed-phase HPLC was performed on a Bio-Rad Hi-pore RP-318 reversed-phase HPLC column {7 mL/min, $HCOO^-(NH_4)^+$ [50 mM, pH 4.7]}.

Enzymatic Synthesis of (E)- and (Z)-EB-UDP-GlcNAc. (*E*)-EB-UDP-GlcNAc and (*Z*)-EB-UDP-GlcNAc were prepared in a manner similar to that reported previously (Lees & Walsh, 1995) with the exception of the HPLC eluent [$HCOO^-(NH_4)^+$ (7 mL/min, 50 mM, pH 4.7)].

Structure Determination of the (E)-EB-UDP-GlcNAc Complex. Crystals of the (*E*)-EB-UDP-GlcNAc complex with the enzyme MurB were grown under conditions similar to those of crystals of the EP-UDP-GlcNAc complex (Benson et al., 1994). A stock solution of (*E*)-EB-UDP-GlcNAc (57 mM) was diluted into a 10 mg/mL solution of MurB in 10 mM Tris-HCl buffer, pH 8.0, to a final substrate concentration of 5.7 mM just prior to crystallization. Crystals were grown in hanging drops at 25 °C in 13−14% PEG 8000, 100 mM HEPES, pH 8.0, and 200 mM calcium acetate and have the same morphology as native crystals and approximate dimensions of 0.2 × 0.2 × 0.1 mm. These crystals belong to the same tetragonal space group as the EP-UDP-GlcNAc complex crystals, $P4_32_12$ with $a = b = 49.7$ Å, $c = 264.3$ Å, and $\alpha = \beta = \gamma = 90°$.

X-ray diffraction data were collected on a single crystal frozen in a stream of liquid nitrogen at −160 °C after being soaked in cryoprotecting buffer (crystallization solution plus 17% glycerol) for 5 min. A Siemens multiwire detector using a Siemens rotating anode X-ray source at 50 kV and 100 mA was used to collect the data in 0.1° steps with a crystal to detector distance of 18.0 cm, various 2θ angles to collect the high-resolution data, and 4 min exposure times. The data were indexed and integrated using the BUDDHA package (Blum et al., 1987). Integrated intensities were grouped into 2° batches for scaling using the programs ROTAVATA and AGROVATA, and structure factor amplitudes were calculated using TRUNCATE from the CCP4 suite (Collaborative Computational Project No. 4, 1994). Data collection statistics are shown in Table 1.

The starting model for the refinement of the (*E*)-EB-UDP-GlcNAc−MurB complex was the EP-UDP-GlcNAc−MurB

complex which had been previously refined to 2.7 Å (Benson et al., 1995). Reflections for the calculation of the free *R* factor (Brünger, 1992a) were equivalent to those used for the EP-UDP-GlcNAc−MurB complex from 8.0 to 2.7 Å with additional reflections chosen randomly in the 2.7−2.3 Å range. Stereochemically constrained positional refinement, simulated annealing, and individual *B* factor refinement were conducted using X-PLOR (Brünger, 1992b). Each round of refinement was followed by manual rebuilding using the program O (Jones et al., 1991). The model for the (*E*)-EB-UDP-GlcNAc substrate was built by adding an additional methyl group onto the EP-UDP-GlcNAc structure from the starting model in the (*E*) conformation. Omit maps alternatively excluding 30 residues at a time, the ligands, or waters were used in the initial and final stages of refinement to check protein, substrate, and solvent models. The solvent model was rebuilt entirely. Only waters which were clearly present in both the $2F_o - F_c$ and $F_o - F_c$ maps and which exhibited reasonable hydrogen-bonding distances, geometry, and occupancies were included. Analysis of the stereochemistry by PROCHECK (Laskowski et al., 1993) showed that 100% of the main-chain torsions fall within the allowed regions of the Ramachandran plot.

Determination of the Reaction Rate of MurB with (Z)-EB-UDP-GlcNAc. MurB (0, 10, or 20 μL; 250 units/mL) was added to 1 mL of a solution of (*Z*)-EB-UDP-GlcNAc (1 mM), NADPH (5 mM), KCl (20 mM), DTT (1 mM), and Tris-HCl (50 mM, pH 8.0). Aliquots of the reaction mixtures (100 μL) were injected onto an analytical reversed-phase column at various times.

Enzymatic Synthesis of [$^2H_2$]-UDP-Me-MurNAc. The procedure outlined in Benson et al. (1993) for the synthesis of NADPD was scaled up. $NADP^+$ (0.214 g, 0.25 μmol), glutathione (0.442 g, 1.4 μmol), DTT (1.48 g, 10 μmol), and triethanolamine (HCl salt, 0.216 g) were dissolved in D_2O (30 mL) and adjusted to pD 9.1. Glutathione reductase (100 μL, 500 units, EC 1.6.4.2, type IV from Bakers' yeast, Sigma G-4759) was then added to the reaction mixture. After 16 h at 25 °C, the reaction mixture was stored at 4 °C for 48 h. (*E*)-EB-UDP-GlcNAc (5 mL of a 18 mM solution in D_2O), KCl (1.5 mL of a 1 M solution in D_2O), and MurB (200 μL, 50 units in H_2O; 21.5 units/mg of enzyme) were then added. After a further 21 h at 25 °C, the reaction mixture was purified by preparative reversed-phase HPLC and then preparative anion-exchange HPLC using routine 1 to provide [$^2H_2$]-UDP-Me-MurNAc (47 μmol). A high-resolution mass spectrum confirmed that the product was [$^2H_2$]-UDP-Me-MurNAc. [HRMS (FAB, $[M - H]^-$), calculated for $C_{21}H_{31}D_2O_{19}N_3P_2$ *m*/*e* 694.1231, found *m*/*e* 694.1226.]

Decomposition of [$^2H_2$]-UDP-Me-MurNAc. [$^2H_2$]-UDP-Me-MurNAc (47 μmol) in D_2O (1 mL) was mixed with 30% NaOD in D_2O (1 mL). After 6 days the reaction mixture was passed over an AG-50W-X8 ion-exchange column (NH_4^+ form, 75 mL). The fractions absorbing at 262 nm were combined, lyophilized, redissolved in D_2O (4 mL), and mixed with 0.4 mL of a 0.1 M Tris (free base) solution in D_2O. Alkaline phosphatase [44 μL, 17.4 units/μL, suspension in 3.2 M $(NH_4)_2SO_4$, EC 3.1.3.1, grade 1 from calf intestines, Boehringer Mannheim 108 146] was added. After 2 h the reaction was complete as determined by ^{1}H NMR spectroscopy. Concentrated NaOD in D_2O (120 μL) was then added (Veyriéres & Jeanloz, 1970). After 3 days the crude sample was compared with authentic (2*R*,3*R*)- and (2*R*,3*S*)-[2,3-$^2H_2$]-2-hydroxybutyrate (*vide infra*) by ^{1}H NMR spectroscopy. The sample was then stirred with AG-50W-X8 resin (H^+ form, 2 mL) for 2 min. The solution was filtered through glass wool, and the resin was washed twice with 2 mL of D_2O. The combined aqueous solution was then extracted six times with 30 mL of diethyl ether. The combined organics were dried over $MgSO_4$, filtered, and back-extracted five times with 3 mL of aqueous NH_4OH (1.5 M). The combined aqueous solutions were lyophilized to provide [2,3-$^2H_2$]-2-hydroxybutyrate (90% purity with residual nucleoside by ^{1}H NMR spectroscopy). A high-resolution mass spectrum confirmed the product was [2,3-$^2H_2$]-2-hydroxybutyrate. [HRMS (CI, $[M + NH_4]^+$), calculated for $C_4H_6D_2O_3$ *m*/*e* 124.0943, found *m*/*e* 124.0948.] The relative stereochemistry at C2 and C3 was determined by comparing this material with authentic (2*R*,3*R*)- and (2*R*,3*S*)-[2,3-$^2H_2$]-2-hydroxybutyrate (*vide infra*). The absolute stereochemistry at C2 was determined using the assays for D- and L-lactate outlined in Bergmeyer (Gawehn & Bergmeyer, 1974; Gutmann & Wahlefeld, 1974). A glycine buffer solution (1 mL, 500 mM) containing hydrazine (400 mM) was mixed with a solution of NAD^+ (0.067 mL, 39 mM), a solution of enzyme [0.05 mL, 625 units of D-lactate dehydrogenase (from *Lactobacillus leichmannii*, EC 1.1.1.28, Sigma, L-3888) or 1250 units of L-lactate dehydrogenase (type XI from rabbit muscle, EC 1.1.1.27, Sigma, L-1254)], and either water (0.05 mL, blank), a solution of racemic 2-hydroxybutyrate [0.05 mL, 50 mM (racemic), standard], or a solution of [2,3-$^2H_2$]-2-hydroxybutyrate (0.05 mL, approximately 25 mM, sample) obtained form the decomposition of [$^2H_2$]-UDP-Me-MurNAc. The absorbances of the blank and sample assays with L-LDH varied only slightly at 5 (A_{340} = 0.04 and 0.02, respectively) and 60 (A_{340} = 0.18 and 0.16, respectively) min in comparison with the standard assay (A_{340} = 1.65 and 2.66 at 5 and 60 min, respectively). To ensure that the sample mixture did not contain an inhibitor for L-LDH, a solution of racemic 2-hydroxybutyrate [0.05 mL, 50 mM (racemic)] was added to the sample assay after 60 min. With D-LDH the A_{340} of the blank did not vary with time. The absorbances of the standard and sample assays did vary with time (A_{340} = 1.45 and 0.82, respectively, at 60 min).

Enzymatic Synthesis of Authentic (2R,3R)- and (2R,3S)-[2,3-$^2H_2$]-2-Hydroxybutyrate. NADD (4(*R*)-[^{2}H]-NADH) was prepared according to the method of Viola et al. (1979) with the exception that all solutions were in D_2O. After the completion of the reaction (10 mL, 20 mM NADD), the crude reaction mixture was filtered through a Centriprep-10 and used without further purification. (3*R*)- and (3*S*)-[3-^{2}H]-2-ketobutyrates were prepared using the ability of pyruvate kinase to selectively exchange the *pro-R* proton of 2-ketobutyrate (Hoving et al., 1983). To prepare (2*R*,3*R*)- and (2*R*,3*S*)-[2,3-$^2H_2$]-2-hydroxybutyrate, 3 mL of (3*R*)- or (3*S*)-[3-^{2}H]-2-ketobutyrate (32 mM) was added to 8 mL of the crude NADD solution along with D-lactate dehydrogenase (100 μL in D_2O, 1650 units, from *L. leichmannii*, Sigma, L-3888). After 1 h the reaction mixture was filtered through a Centriprep-3 and extracted in a manner similar to that reported above for the decomposition of [$^2H_2$]-UDP-Me-MurNAc.

MurB-Catalyzed Reduction of (E)-EB-UDP-GlcNAc by NADPH in H_2O and D_2O. Two identical reactions were set up in parallel in H_2O and D_2O. Tris (55 mg of free base),

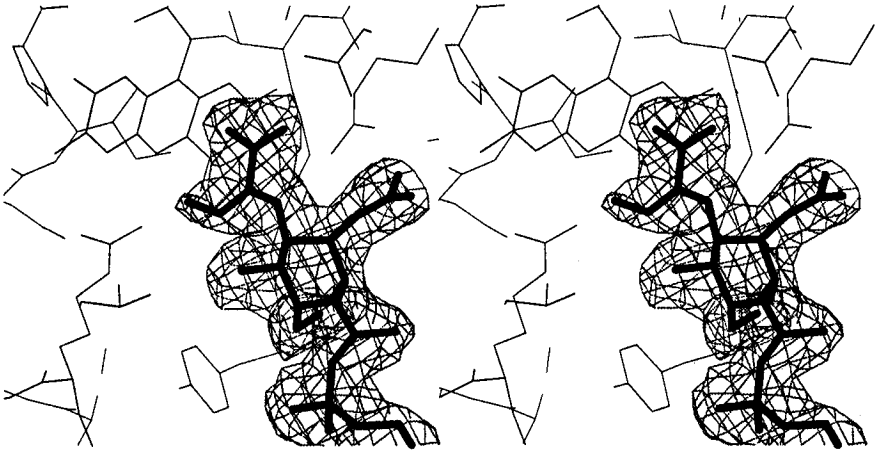

FIGURE 4: Omit difference density for the (*E*)-enolbutyryl-*N*-acetylglucosamine pyrophosphate portion of the (*E*)-EB-UDP-GlcNAc substrate. The map was calculated including data from 12 to 2.3 Å and contoured at 0.7σ.

(*E*)-EB-UDP-GlcNAc (1 mL, 44 μmol), KCl (1 M, 0.18 mL), DTT (0.1 M, 0.09 mL), and NADPH (60 mg, 64 μmol) were mixed together with H_2O or D_2O (7.55 mL). The pH or pD of each of these solutions was adjusted to 8.0 with 1 M HCl or DCl, respectively. MurB (90 μL in H_2O, 22 units) was then added to each reaction mixture. After 24 h, a 1 mL aliquot was removed from each reaction mixture and lyophilized. An NMR spectrum was acquired of each pellet. A portion of each reaction mixture was purified by preparative reversed-phase HPLC and preparative ion-exchange HPLC using routine 2 to provide UDP-Me-MurNAc and [^{2}H]-UDP-Me-MurNAc (with the exception of the small amount of dideuteration in the sample derived from the reaction in D_2O): ^{1}H NMR (D_2O) δ 7.95 (d, 1H, H6″, J = 8.1 Hz), 5.96 (m, 1H, H1), 5.95 (d, 1H, H5″, J = 8.3 Hz), 5.62 (dd, 1H, H1′, J = 7.3, 3.0 Hz), 4.36−4.33 (m, 2H, H2, H3), 4.26 (pentet, 1H, H4, J = 2.5 Hz), 4.20 (ddd, 1H, H5a, J = 11.8, 4.5, 2.5 Hz), 4.18−4.13 (m, 1H, H5b), 4.15 (dd, 1H, H2 of butyl ether, J = 6.6, 5.2 Hz), 3.88 (ddd, 1H, H5′, J = 10.1, 3.9, 2.4 Hz), 3.84 (dt, 1H, H2′, J = 10.8, 2.5 Hz), 3.81 (dd, 1H, H6′a, J = 12.2, 2.2 Hz), 3.76 (dd, 1H, H6′b, J = 12.5, 4.2 Hz) 3.76 (dd, 1H, H3′, J = 10.8, 9.0 Hz), 3.60 (dd, 1H, H4′, J = 9.9, 9.2 Hz), 2.03 (s, 3H, Ac), 1.74−1.62 (m, 2H, H3 of butyl ether), 0.89 (t, 3H, H4 of butyl ether, J = 7.5 Hz); ^{13}C NMR (D_2O) 181.8, 175.5, 167.6, 153.1, 142.7, 103.8, 94.9 (d, J = 6.8 Hz), 89.4, 84.3 (d, J = 9.2 Hz), 83.7, 78.1, 74.8, 74.2, 70.8, 70.3, 66.0 (d, J = 4.9 Hz), 61.3, 54.1 (d, J = 8.4 Hz), 27.3, 23.2, 10.2 ppm. [HRMS (FAB, [M − H]$^-$), calculated for $C_{21}H_{33}O_{19}N_3P_2$ *m/e* 692.1105, found *m/e* 692.1077.] (*Z*)-EB-UDP-GlcNAc was purified in a similar manner to the purification of UDP-Me-MurNAc described above. The ^{1}H NMR and mass spectra of the isolated (*Z*)-EB-UDP-GlcNAc were in agreement with authentic material (Lees & Walsh, 1995) (with the exception of the small amount of deuteration in the sample derived from the reaction in D_2O).

RESULTS

Structure Determination of the (E)-EB-UDP-GlcNAc Complex. Crystals of the (*E*)-EB-UDP-GlcNAc−MurB complex diffracted to 2.3 Å at −160 °C. The current model for 340 residues, FAD, (*E*)-EB-UDP-GlcNAc, and 119 water molecules was refined to 2.3 Å with a crystallographic *R* factor of 23.8% for all data. Residues 1 and 2 were disordered as they were in the EP-UDP-GlcNAc complex. A difference map at 3.0 Å clearly revealed positive difference density in the active site adjacent to C3 of the enolbutyryl moiety, consistent with the extra methyl group in the enolbutyryl substrate in the (*E*)-conformer. Omit difference density for the (*E*)-EB-UDP-GlcNAc substrate confirmed this assignment of the (*E*)-isomer (Figure 4). This result corroborates the NMR-derived assignment of the (*E*)-isomer (Lees & Walsh, 1995).

The rms deviation of C_α between the EP-UDP-GlcNAc complex solved and refined to 2.7 Å and the (*E*)-EB-UDP-GlcNAc complex at 2.3 Å is 0.38 Å. Within the active site several changes occur upon binding of the (*E*)-EB-UDP-GlcNAc substrate. In the (*E*)-EB-UDP-GlcNAc complex rotations of +4° around the C2−C3 bond and −4° around the C1−C2 bond of the ribityl sugar of the FAD occur with respect to their orientation as in the EP-UDP-GlcNAc complex. These rotations in the ribityl sugar result in a concerted movement of the isoalloxazine ring system by 0.9 Å to accommodate the additional methyl group of the (*E*)-EB substrate. This shift repositions the N5 of the flavin between the C3−C4 bond of the (*E*)-EB-UDP-GlcNAc substrate as opposed to directly over C3 in the EP-UDP-GlcNAc−MurB complex (Figure 5a, b). This movement brings Arg-214 within 3.0 Å of N5, which is close enough for hydrogen bonding to stabilize either the reduced or oxidized flavin as suggested previously (Benson et al., 1995). The location of the methyl group at C3 in the (*E*)-isomer of the enolbutyrate partially fills a hydrophobic pocket bounded by Leu-218 and the dimethyl benzene ring of the flavin (Figure 5b).

Stereochemistry of MurB. Both (*E*)- and (*Z*)-EB-UDP-GlcNAc served as substrates for MurB. The rate constant for reduction of (*E*)-EB-UDP-GlcNAc (substrate concentration of 1 mM) was 100-fold less than the rate constant for reduction of EP-UDP-GlcNAc (k_{cat} = 1300 min^{-1}), while the rate constant for reduction of (*Z*)-EB-UDP-GlcNAc (substrate concentration of 1 mM) was 10 000-fold less than the rate constant for reduction of EP-UDP-GlcNAc. The difference between rate constants for reduction of (*E*)- and (*Z*)-EB-UDP-GlcNAc may be due to the 40-fold greater thermodynamic stability of (*Z*)-EB-UDP-GlcNAc relative to (*E*)-EB-UDP-GlcNAc (Lees & Walsh, 1995).

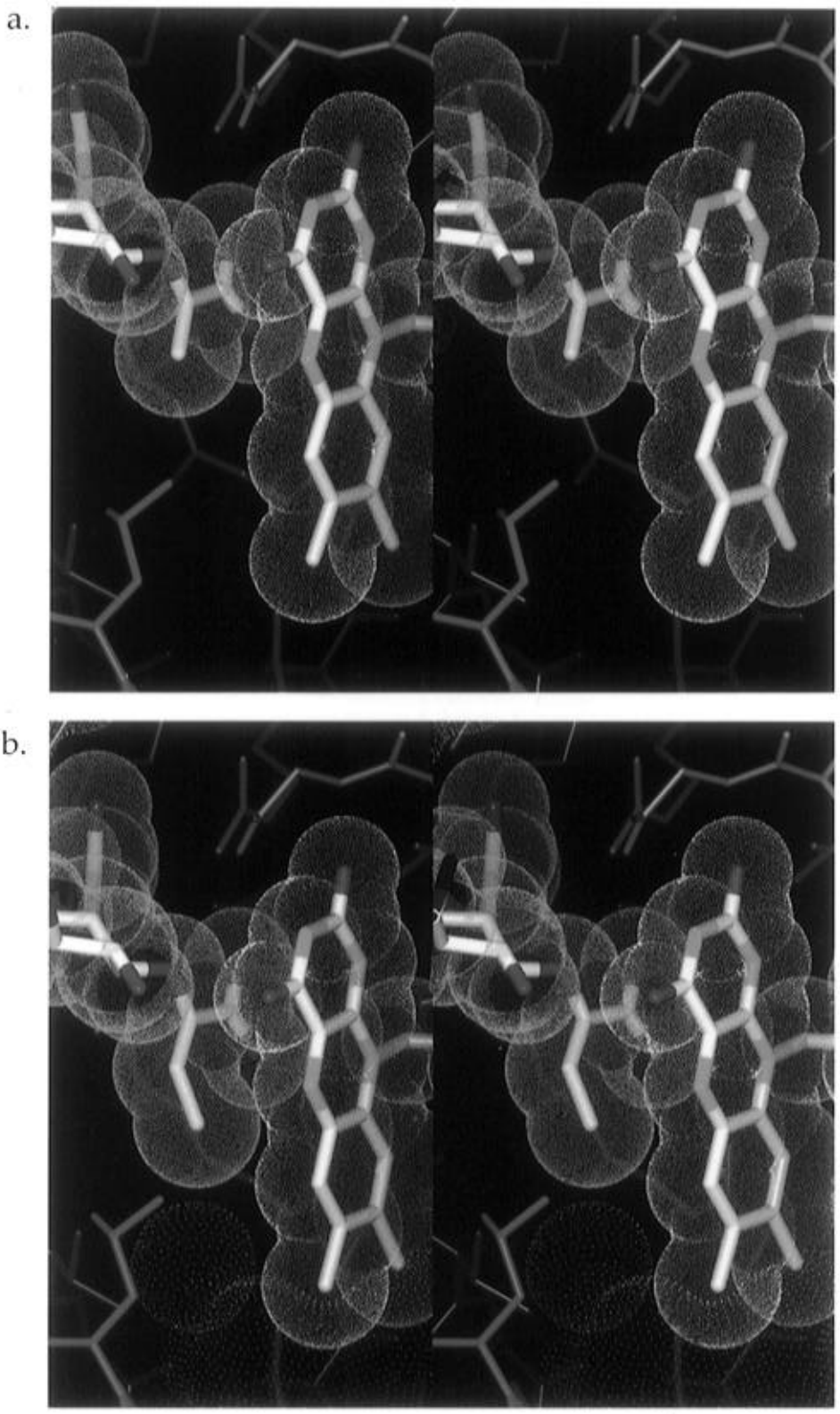

FIGURE 5: (a) Active site of the EP-UDP-GlcNAc−MurB complex showing the van der Waals surface for the FAD cofactor (yellow) and the EP-UDP-GlcNAc substrate (cyan). The enolpyruvyl moiety can be seen with the carboxylate group lying under the FAD. The C3 of the enolpyruvyl moiety lies directly across from N5 of the flavin. Leu-218 (magenta) forms a hydrophobic pocket with the dimethylbenzene ring of the FAD. (b) Active site of the (*E*)-EB-UDP-GlcNAc−MurB complex showing the van der Waals surface for the FAD cofactor (yellow) and the (*E*)-EB-UDP-GlcNAc substrate (cyan). The movement of the FAD can be seen by noting the positioning of N5 of the FAD between the C3 and C4 atoms of the enolbutyryl moiety. Movement of Leu-218 (magenta) along with the flavin has created a solvent-accessible pocket (Connolly, 1983a,b) next to C4 of the (*E*)-EB-UDP-GlcNAc (white).

To determine the stereochemistry of enzymatic addition of hydride at C3 of the enol ether substrate, it was necessary to synthesize a product using MurB that was chiral at C3 and convert that product to a compound of known chirality. MurB catalyzed the reduction of (*E*)-EB-UDP-GlcNAc with NADPD in D_2O to [2,3-$^2H_2$]-UDP-Me-MurNAc. This product was decomposed in three steps to [2,3-$^2H_2$]-2-hydroxybutyrate (Figure 6), a compound that retained the

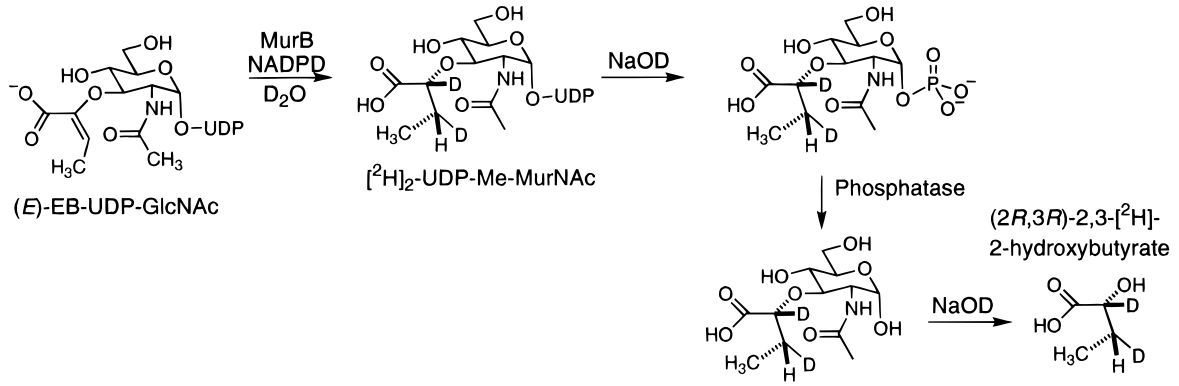

FIGURE 6: Experimental strategy for stereochemical analysis of the MurB reaction.

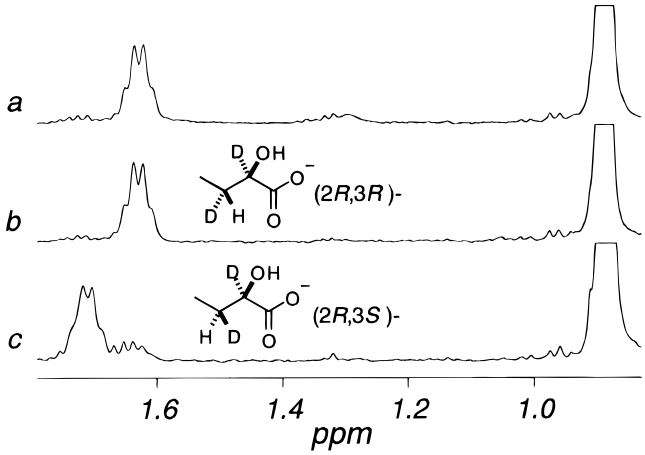

FIGURE 7: ^{1}H NMR spectra of (a) [2,3-$^2H_2$]-2-hydroxybutyrate obtained from the decomposition of [$^2H_2$]-UDP-Me-MurNAc, (b) authentic (2*R*,3*R*)-[2,3-$^2H_2$]-2-hydroxybutyrate obtained using pyruvate kinase, or (c) authentic (2*R*,3*S*)-[2,3-$^2H_2$]-2-hydroxybutyrate obtained using pyruvate kinase. Spectrum c contains about 25% [2-^{2}H]-2-hydroxybutyrate. All spectra were taken in 0.1 M phosphate-buffered D_2O (0.05 M NaH_2PO_4, 0.05 M Na_2HPO_4).

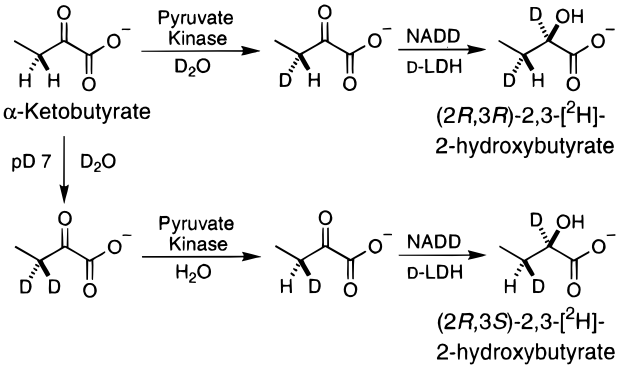

FIGURE 8: Synthesis of (2*R*,3*R*)- and (2*R*,3*S*)-[2,3-$^2H_2$]-2-hydroxybutyrate using pyruvate kinase.

two chiral centers at C2 and C3 in their original form. The absolute stereochemistry at C2 was determined to be (*R*) as the [2,3-$^2H_2$]-2-hydroxybutyrate was a substrate for D-LDH but not for L-LDH (Gawehn & Bergmeyer, 1974; Gutmann & Wahlefeld, 1974). The relative stereochemistry between C2 and C3 was determined by comparing the ^{1}H NMR spectrum of the [2,3-$^2H_2$]-2-hydroxybutyrate with the spectrum of each diastereomer of (2*R*)-[2,3-$^2H_2$]-2-hydroxybutyrate (Figure 7). Both diastereomers were synthesized using pyruvate kinase which selectively exchanges the *pro-R* hydrogen of 2-ketobutyrate with solvent protons (Hoving et al., 1983) (Figure 8). Given the absolute stereochemistry at C2 and the relative stereochemistry between C2 and C3 (Figure 7), the stereochemistry of the [2,3-$^2H_2$]-2-hydroxybutyrate is unambiguously (2*R*,3*R*). The stereochemistry of the original [2,3-$^2H_2$]-UDP-Me-MurNAc is thus also (2*R*,3*R*).

MurB-Catalyzed Isomerization of (E)-EB-UDP-GlcNAc to (Z)-EB-UDP-GlcNAc. During the conversion of (*E*)-EB-UDP-GlcNAc to UDP-Me-MurNAc, the formation of the isomeric (*Z*)-EB-UDP-GlcNAc was observed. To further characterize the isomerization of (*E*)- to (*Z*)-EB-UDP-GlcNAc, the MurB-catalyzed reduction of (*E*)-EB-UDP-GlcNAc with NADPH was performed in parallel in D_2O and H_2O. The ratio of (*Z*)-EB-UDP-GlcNAc to UDP-Me-MurNAc product was greater by a factor of 1.8 in D_2O (16:84) than in H_2O (9:91) (Figure 9), reflecting a product-determining isotope effect. The ratio of (*Z*)-EB-UDP-GlcNAc to UDP-Me-MurNAc product in D_2O was constant as a function of percent conversion and was not affected by shifting the pD of the reaction by 0.5 unit in either direction.

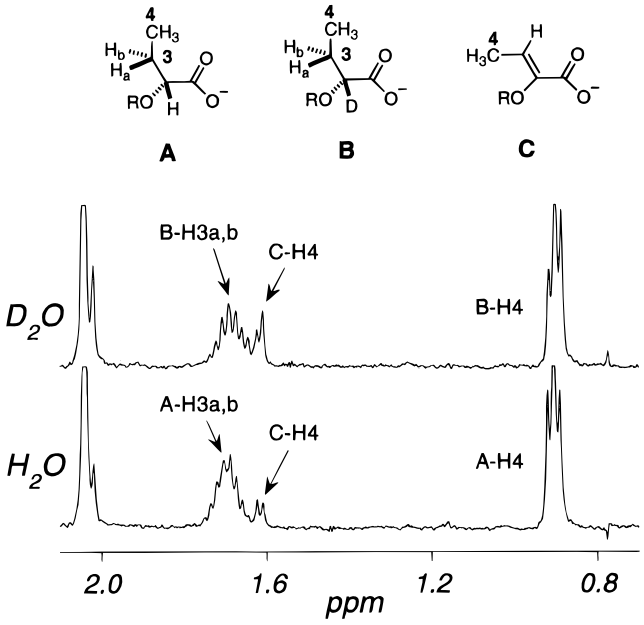

FIGURE 9: ^{1}H NMR spectra of the MurB-catalyzed reduction of (*E*)-EB-UDP-GlcNAc with NADPH in D_2O and H_2O at completion. The ratio of (*Z*)-EB-UDP-GlcNAc (compound **C**) to UDP-Me-MurNAc (compounds **A** and **B**) was obtained from the average of the relative integrals of the two *N*-acetyl peaks at 2.0 ppm and the relative integrals of the two CH_3 peaks.

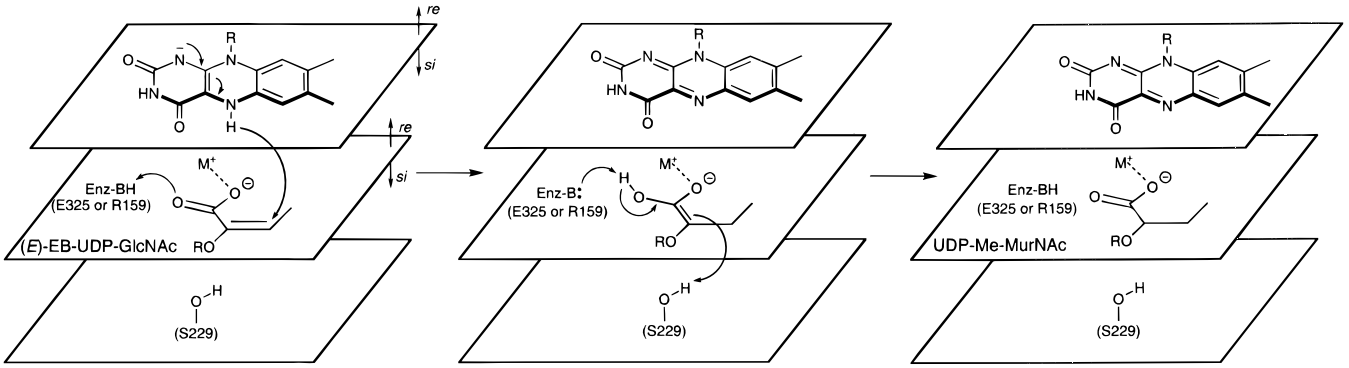

FIGURE 10: Proposed mechanism for MurB-catalyzed reduction of (*E*)-EB-UDP-GlcNAc.

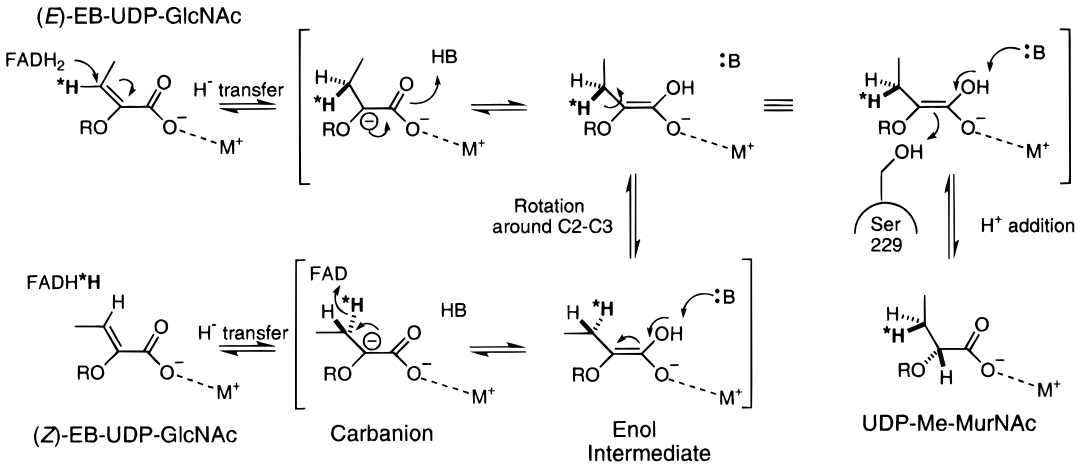

FIGURE 11: (*E*)- to (*Z*)-isomerization via a carbanion/enol intermediate.

The UDP-Me-MurNAc product isolated from the reaction performed in D_2O with NADPH was a mixture of C2-[^{2}H] and C2,C3-[$^2H_2$]-product (in a ratio of 3:1, Table 2). The (*Z*)-EB-UDP-GlcNAc isolated from the same reaction was a mixture of nondeuterated and C3-[^{2}H]-(*Z*)-EB-UDP-GlcNAc (3:1).

DISCUSSION

(E)-EB-UDP-GlcNAc Binding to MurB. The crystal structure of (*E*)-EB-UDP-GlcNAc bound to MurB was similar to that of the natural substrate EP-UDP-GlcNAc bound to MurB. The slight differences at the active site included an in-plane shift of N5 of the FAD away from C3 of the bound substrate which allows accommodation of the additional enolbutyrylmethyl group. As a result of this shift, N5 is no longer positioned directly above C3 as it is for the natural substrate EP-UDP-GlcNAc. The displacement of N5 relative to C3 is a possible factor in the 100-fold decreased rate constant for reduction of the (*E*)-EB-UDP-GlcNAc compared to EP-UDP-GlcNAc.

Stereochemistry of Reduction of (E)-EB-UDP-GlcNAc. In the reductive saturation of the enol ether C2−C3 double bond of the normal substrate EP-UDP-GlcNAc, the stereochemical outcome at C3 is cryptic in the torsiosymmetric methyl group of the UDP-MurNAc product. To address mechanistic predictions from the X-ray crystal structures of both the EP- and (*E*)-EB-UDP-GlcNAc enzyme complexes, the stereochemistry of reduction at C3 was determined using (*E*)-EB-UDP-GlcNAc. (*E*)-EB-UDP-GlcNAc is reduced by MurB to UDP-Me-MurNAc, a product with a prochiral group at the C3 locus. Deuterium substitution of either prochiral hydrogen would yield a (3*R*)- or (3*S*)-[^{2}H] product. In this work reduction was performed with NADPD in D_2O, yielding UDP-Me-MurNAc fully deuterated at C3 as well as C2. This [$^2H_2$]-UDP-Me-MurNAc product was decomposed in three steps involving UMP elimination, phosphate hydrolysis, and ether elimination (Figure 6). The resulting [2,3-$^2H_2$]-2-hydroxybutyrate was cleanly determined to be (2*R*,3*R*)-[2,3-$^2H_2$]-2-hydroxybutyrate on the basis of its ability to be oxidized by NAD^+ in the presence of D-LDH but not L-LDH and by comparison with enzymatically synthesized

Table 2: Relative Mass Spectral Intensities and Approximate Deuterium Content of (*Z*)-EB-UDP-GlcNAc and UDP-Me-MurNAc Products[a]

		relative intensities[b]			approx
product	reaction	M	M + 1	M + 2	excess % D
(*Z*)-EB-UDP-GlcNAc	in H_2O	100	31.7		0
	in D_2O	100	69.5		27
UDP-Me−MurNAc	in H_2O	100	26.4		0
	in D_2O		100	58.0	24[c]

[a] The reaction conditions are described in Experimental Procedures. [b] The mass was determined by negative ion FAB-MS, and M corresponds to the [(perprotio molecular mass) − H]$^-$ peak. The highest intensity peak was assigned a value of 100. [c] The expected product from this reaction is the monodeuterated UDP-Me-MurNAc, and therefore any dideuterated UDP-Me-MurNAc is recorded as excess deuteration.

(2*R*,3*R*)- and (2*R*,3*S*)-[2,3-$^2H_2$]-2-hydroxybutyrate standards (Figure 7). Thus the H^-/H^+ addition catalyzed by MurB was determined to be *anti*. This result confirms the mechanistic prediction from the X-ray crystal structure of the (*E*)-EB-UDP-GlcNAc−MurB complex that hydride transfer at C3 is to the *re* face (determined from C2) of the enolbutyryl group (Figure 10). Given the similarities in the crystal structures of (*E*)-EB-UDP-GlcNAc and EP-UDP-GlcNAc bound to MurB, hydride transfer at C3 is also to the *re* face (determined from C2) of the enolpyruvyl group (Benson et al., 1995). The (2*R*) stereochemistry of UDP-Me-MurNAc is the same as the stereochemistry at C2 of MurNAc (Veyriéres & Jeanloz, 1970).

Mechanistic Implications: Substrate Reduction. The enzymatic reduction of (*E*)-EB-UDP-GlcNAc in D_2O with NADPH produced both C2-[^{2}H]- and C2,C3-[$^2H_2$]-UDP-Me-MurNAc in a 3:1 ratio (Table 2). The predominant appearance of the C2-[^{2}H] product clearly indicates that the proton at C3 is derived from NADPH and the proton at C2 is derived from a solvent-accessible source. This transfer of hydrogens is similar for the natural substrate, EP-UDP-GlcNAc, where the C2 and C3 protons are also derived from NADPH and solvent, respectively (Benson et al., 1993). The unexpected production of the minor [$^2H_2$] product is probably due to the exchange of the N5-H of the reduced flavin ($FADH_2$) with solvent protons. Solvent exchange of the proton at N5 of $FADH_2$ has been observed with other flavoproteins (Walsh, 1980). However, with the natural substrate EP-UDP-GlcNAc, the proton at N5 of the FAD does not exchange within the limits of detection (±5%) (Benson et al., 1993) despite the fact that the N5 of the FAD is equally accessible to solvent in the EP-UDP-GlcNAc−MurB and (*E*)-EB-UDP-GlcNAc−MurB crystal structures (Benson et al., 1995). The differences observed in solvent proton incorporation into the product at C3 are probably due to the 100-fold slower overall reaction rate of the (*E*)-EB-UDP-GlcNAc. The slower reaction rate allows the enzyme to exist in the $FADH_2$ state for a longer time, increasing the possibility of solvent exchange before reoxidation via hydride transfer to bound enol ether substrate occurs.

Mechanistic Implications: Substrate Isomerization. During the reduction of (*E*)-EB-UDP-GlcNAc to UDP-Me-MurNAc by MurB, the generation of (*Z*)-EB-UDP-GlcNAc was observed, reflecting a partitioning between enol ether reduction and geometric isomerization. The reaction in D_2O with NADPH produced predominantly perprotio-(*Z*)-EB-UDP-GlcNAc, demonstrating that the C3 proton was derived from NADPH as opposed to solvent which would have generated a C3-[^{2}H]-(*Z*)-EB-UDP-GlcNAc. The small amount of C3-[^{2}H]-(*Z*)-EB-UDP-GlcNAc produced during the reaction is postulated to be due to the exchange of solvent protons with the reduced FAD. Because the proton at C3 is derived from NADPH, the (*Z*)-EB-UDP-GlcNAc can only arise via an intermediate with sp^3 geometry at C3. (*Z*)-EB-UDP-GlcNAc was not derived from the back-reaction of UDP-Me-MurNAc because the ratio of (*Z*)-EB-UDP-GlcNAc to UDP-Me-MurNAc remained a constant during the course of the reaction. Thus the net (*E*)- to (*Z*)-EB-UDP-GlcNAc conversion is postulated to occur by the initial formation of a carbanion/enol intermediate by hydride addition to C3 of (*E*)-EB-UDP-GlcNAc, followed by rotation about the C2−C3 bond, and subsequent hydride elimination back to FAD (Figure 11). This reversible hydride transfer to and from C3 with intervening single bond rotation in kinetic competition with C2 protonation strongly implicates a relatively long lived C2 carbanion/enol intermediate.

The ratio of products from the action of MurB on (*E*)-EB-UDP-GlcNAc is dependent on the isotopic content of the solvent. The proposed mechanism for MurB (Figure 11) predicts that the carbanion/enol intermediate can partition either to (*Z*)-EB-UDP-GlcNAc or UDP-Me-MurNAc. The formation of (*Z*)-EB-UDP-GlcNAc involves the transfer, after C2−C3 rotation, of a hydride originally present in the C3 position of (*E*)-EB-UDP-GlcNAc, while the formation of UDP-Me-MurNAc involves the transfer to C2 of a solvent-derived proton. In D_2O, the hydride transfer will be unaffected, but the protonation process, which involves a solvent-derived proton, should be susceptible to retardation by a solvent deuterium isotope effect. The net effect should be to bias the partitioning selectively toward the formation of (*Z*)-EB-UDP-GlcNAc, and this expectation is observed with a 1.8-fold increase in the ratio of (*Z*)-EB-UDP-GlcNAc to UDP-Me-MurNAc in D_2O as compared to H_2O.

The ratio of (*Z*)-EB-UDP-GlcNAc to UDP-Me-MurNAc is independent of the hydrogen isotope being transferred from $FADH_2$ to (*E*)-EB-UDP-GlcNAc. The hydride derived from $FADH_2$ is not involved in either the hydride transfer from the carbanion/enol intermediate to FAD generating (*Z*)-EB-UDP-GlcNAc or the protonation of the carbanion/enol intermediate to form UDP-Me-MurNAc (Figure 11). Because the hydride derived from $FADH_2$ is involved in neither of the partitioning steps, the product ratio should be unaffected. Experimentally, the $FADH_2$ that has exchanged *in situ* with D_2O, generating FADHD, partitions with a similar ratio as the $FADH_2$ that has not exchanged with solvent, as determined by the similar excess deuterium content of both (*Z*)-EB-UDP-GlcNAc and UDP-Me-MurNAc (Table 2). This lack of a hydride transfer product-determining isotope effect and the observation of a solvent product-determining isotope effect thus provide further evidence for a long-lived carbanion equivalent that partitions as in Figure 11.

ACKNOWLEDGMENT

We thank Dennis H. Kim and Gregory W. Tucker-Kellogg for their helpful comments. We also thank members of the Walsh group for comments on the manuscript.

REFERENCES

Benson, T. E., Marquardt, J. L., Marquardt, A. C., Etzkorn, F. A., & Walsh, C. T. (1993) *Biochemistry 32*, 2024−2030.

Benson, T. E., Walsh, C. T., & Hogle, J. M. (1994) *Protein Sci. 3*, 1125−1127.

Benson, T. E., Filman, D. J., Walsh, C. T., & Hogle, J. M. (1995) *Nat. Struct. Biol. 2*, 644−653.

Blum, M., Metcalf, P., Harrison, S. C., & Wiley, D. C. (1987) *J. Appl. Crystallogr. 20*, 235−242.

Brown, E. D., Vivas, E. I., Walsh, C. T., & Kolter, R. (1995) *J. Bacteriol. 177*, 4194−4197.

Brünger, A. T. (1992a) *Nature 355*, 472−475.

Brünger, A. T. (1992b) *X-PLOR version 3.1: A System for X-ray Crystallography and NMR*, Pages, Yale University Press, New Haven, CT.

Collaborative Computational Project No. 4 (1994) *Acta Crystallogr. D50*, 760−763.

Connolly, M. L. (1983a) *J. Appl. Crystallogr. 16*, 548−558.
Connolly, M. L. (1983b) *Science 221*, 709−713.
Dhalla, A. M., Yanchunas, J., Ho, H. T., Falk, P. J., Villafranca, J. J., & Robertson, J. G. (1995) *Biochemistry 34*, 5390−5402.
Gawehn, K., & Bergmeyer, H. U. (1974) in *Methods of Enzymatic Analysis* (Bergmeyer, H. U., Ed.) pp 1492−1495, Academic Press, Inc., New York.
Gutmann, I., & Wahlefeld, A. W. (1974) in *Methods of Enzymatic Analysis* (Bergmeyer, H. U., Ed.) pp 1464−1468, Academic Press, Inc., New York.
Hoving, H., Nowak, T., & Robillard, G. T. (1983) *Biochemistry 22*, 2832−2838.
Jones, T. A., Zou, J.-Y., Cowan, S. W., & Kjeldgaard, M. (1991) *Acta Crystallogr. A47*, 110−119.
Laskowski, R. A., MacAurthur, M. W., Moss, D. S., & Thorton, J. M. (1993) *J. Appl. Crystallogr. 26*, 283−291.
Lees, W. J., & Walsh, C. T. (1995) *J. Am. Chem. Soc. 117*, 7329−7337.
Veyriéres, A., & Jeanloz, R. W. (1970) *Biochemistry 9*, 4153−4159.
Viola, R. E., Cook, P. F., & Cleland, W. W. (1979) *Anal. Biochem. 96*, 334−340.
Walsh, C. T. (1980) *Acc. Chem. Res. 13*, 148−155.

BI952287W